Electron backscatter diffraction and electron channeling contrast imaging of tilt and dislocations in nitride thin films

C. Trager-Cowan and F. Sweeney
SUPA, Department of Physics, University of Strathclyde, Glasgow G4 ONG, Scotland, United Kingdom

P. W. Trimby, A. P. Day, A. Gholinia, and N.-H. Schmidt
HKL TECHNOLOGY A/S, Majsmarken 1, Hobro, DK 9500, Denmark

P. J. Parbrook
EPSRC National Centre for III-V Technologies, University of Sheffield, United Kingdom

A. J. Wilkinson
Department of Materials, University of Oxford, Oxford OX1 3PH, United Kingdom

I. M. Watson
SUPA, Institute of Photonics, University of Strathclyde, Glasgow G4 ONW, Scotland, United Kingdom
(Received 12 June 2006; published 1 February 2007)

In this paper we describe the use of electron backscatter diffraction (EBSD) mapping and electron channeling contrast imaging—in the scanning electron microscope—to study tilt, atomic steps and dislocations in epitaxial GaN thin films. We show results from a series of GaN thin films of increasing thickness and from a just coalesced epitaxial laterally overgrown GaN thin film. From our results we deduce that EBSD may be used to measure orientation changes of the order of 0.02°, in GaN thin films. As EBSD has a spatial resolution of ≈20 nm, this means we have a powerful technique with which to quantitatively map surface tilt. We also demonstrate that electron channeling contrast images may be used to image tilt, atomic steps, and threading dislocations in GaN thin films.

DOI: 10.1103/PhysRevB.75.085301 PACS number(s): 68.55.Jk, 68.37.Hk, 61.72.Ff, 61.82.Fk

I. INTRODUCTION

A. Nitrides

Nitride thin films are used in the manufacture of UV/blue laser diodes, UV/visible LEDs, and white LEDs. Nitride laser diodes are presently dictating developments of DVDs, printing, and color copying, and present applications of nitride LEDs extend from street lighting, to back lighting in mobile phones, to traffic lights.[1,2] Future use of nitride-based LEDs promises to revolutionize lighting in the home and office. Nitrides are also being developed for the production of high frequency, high power electronic devices.[3,4]

Even though commercial devices are available, the quality of nitride thin films and subsequent devices (Ref. 5 and references therein) is variable due to the mismatch between the epitaxial nitride thin films and presently used substrates. Dislocation densities in bulk epitaxial GaN thin films can range from 10^8 to 10^{10} cm^{-2} (Ref. 6).

B. Electron backscatter diffraction

Electron backscatter diffraction (EBSD) in the scanning electron microscope (SEM) is an attractive technique with which to interrogate the crystallographic properties of nitride thin films because it can provide information on crystal orientation, polytype, and strain with a resolution of around 20 nm.[7] In electron backscatter diffraction an electron beam is incident on a sample which is tilted at an angle typically ≥70°. The impinging electrons are scattered inelastically through high angles forming a diverging source of electrons that can be diffracted. A simple description for the formation of EBSD patterns presumes that electrons that satisfy the Bragg condition for a given plane emanate in diffraction cones from both the upper and lower surfaces of that plane. When these cones intersect the phosphor screen Kikuchi lines are observed[8] [see Figs. 1(a)–1(c)]. The Kikuchi lines appear as almost straight lines because the cones are very shallow, as the Bragg angle θ_D is of order 1°. Each Kikuchi band is effectively the trace of the plane from which it is formed; an EBSD pattern thus provides a direct measurement of a sample's crystal structure as it is a two-dimensional (2D) projection (the gnomonic projection) of the crystal structure. Rotation of a crystal will produce a rotation of the EBSD pattern; a tilt of a crystal will produce a shift in the EBSD pattern. EBSD patterns acquired from a mesh of points on a sample can be used to produce a map of tilt or rotations in that sample.

To date EBSD has predominantly been applied in metallurgy[9] and in geology,[10] being applied to the measurement of texture,[11] and for the identification of different crystalline phases. Wilkinson[12] and Troost *et al.*[13] have applied EBSD to the measurement of strain in SiGe epilayers, while Baba-Kishi[14] has used EBSD to investigate crystallographic polarity in noncentrosymmetric materials. In nitrides EBSD has been used to measure the orientation between nitride thin films and their substrates and measure tilt in nitride thin films[15] and to identify zinc blende inclusions in a predominantly wurtzite film.[16] EBSD has also been applied to the

 ©2007 The American Physical Society

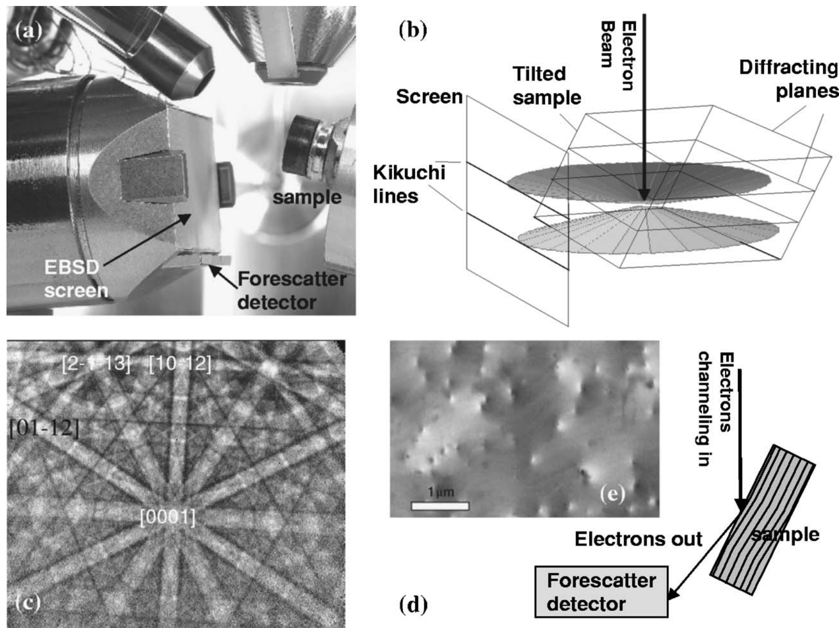

FIG. 1. (a) HKL Technology EBSD and forescatter detector. (b) Schematic diagram illustrating formation of EBSD patterns. (c) Example EBSD pattern from wurtzite GaN. (d) Schematic diagram illustrating formation of electron channeling contrast images. (e) Example electron channeling contrast image from wurtzite GaN thin film. (The "spots" correspond to threading dislocations.)

measurement of strain in nitride films, in particular to investigate lateral variations in strain in epitaxially laterally overgrown GaN (ELOG) films.[16] EBSD may be also combined with other analytical techniques in the SEM, e.g., EDX (Ref. 17) and cathodoluminescence.[16] In this paper we describe its use in conjunction with electron channeling contrast imaging.

C. Electron channeling contrast imaging

In electron channeling contrast imaging the intensity of backscattered electrons depends on the relative orientation of planes in a crystal, so changes in crystallographic orientation (tilt) or changes in lattice constant due to strain are revealed by changes in grey scale in the image. A quantitative analysis of crystallographic orientation from electron channeling image contrast is generally not possible as the same backscattered electron intensity can be generated by several crystal orientations. However, small orientation changes are detectable, allowing the imaging of dislocations for example. Dislocations are imaged due to lattice plane tilting and strain in the vicinity of the dislocations (see for example Refs. 18–23).

There are various names given to the imaging techniques which utilize electron channeling contrast in the scanning electron microscope (SEM). Electron channeling contrast imaging (ECCI) is the name usually given to the technique when images are formed following careful alignment of the channeling crystal planes following the acquisition of an electron channeling contrast pattern (ECP). The acquisition of an ECP allows the g vector of the incident electron beam to be determined.[21] To obtain an ECP in the SEM it is necessary to record changes in backscattered electron intensity as the incident electron beam is rocked through a range of angles relative to the crystal planes. This can be achieved by (1) observing the sample at low magnification, where scanning the beam varies its angle with respect to the sample as well as its position; (2) modifying the SEM electron optics and the current to the scanning coils in order to rock the beam.[21] The second method allows ECPs to be acquired from small (of order microns) regions of the sample. The ECCI technique and its history is summarized in the review paper of Wilkinson and Hirsch.[21]

The acquisition of an ECP and subsequent alignment of the sample is necessary for optimum contrast and the quantitative analysis of electron channeling contrast images. However, images exhibiting channeling contrast can be obtained by the detection of backscattered electrons emanating at a shallow angle from the surface of a sample tilted by around 70°, i.e., the same sample geometry as used for EBSD [see Figs. 1(a), 1(d), and 1(e)]. Tilting the sample increases backscattered electron (BSE) yield, reduces multiple scattering and energy loss processes, thus leading to enhanced channeling contrast.[21] Images obtained without prior alignment of the sample using an ECP are referred to in the literature as electron channeling contrast images or forescatter images (due to the position of the backscattered electron detector(s), which in this geometry are referred to as a forescatter detector(s) [see Figs. 1(a) and 1(d)]) or, for obvious reasons, orientation contrast images.[24–26] As electron channeling contrast imaging is the most descriptive name for the mechanism which produces these images, this is the nomenclature we will use in this paper.

Electron channeling contrast imaging has been applied to the imaging of dislocations and strain fields in both metals and semiconductors and the imaging of orientation variations in geological samples.[18–25] In this paper we demonstrate that electron channeling contrast imaging can be used to image tilt, atomic steps, and threading dislocations in GaN thin films.

II. SAMPLES

In the present work EBSD and electron channeling contrast imaging were used to interrogate a series of five GaN

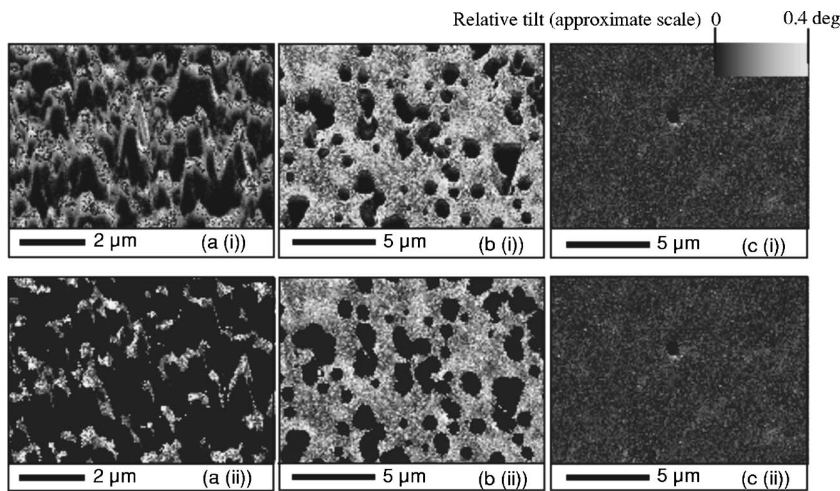

FIG. 2. (a) EBSD tilt map from a 70 nm GaN thin film. (b) EBSD tilt map from a 520 nm GaN thin film. (c) EBSD tilt map from a 1600 nm GaN thin film. The grey scale represents tilt away from the ideal ⟨0001⟩ orientation (in degrees). (i) shows the EBSD tilt maps overlying the EBSD pattern quality. As the EBSD pattern quality is dependent on sample topography, it provides an estimate of the sample topography. (ii) shows the EBSD tilt maps with the EBSD pattern quality information removed.

thin films of increasing thickness from 70 nm to 1600 nm and a just coalesced epitaxial laterally overgrown GaN (ELOG) thin film.

The GaN thin films of increasing thickness were grown by MOVPE using a Thomas Swan Showerhead reactor. For each thin film a 30 nm GaN nucleation layer was first grown at 525 °C on basal plane oriented sapphire substrates. This nucleation layer was then annealed briefly at a GaN growth temperature of 1023 °C prior to thin film growth.

The ELOG film was grown in an Aixtron 200/4 RF-S MOCVD reactor under similar conditions as reported previously.[27] The sample studied consists of a (0001) sapphire substrate on which a 2.5 μm planar seed layer was grown. Over the seed layer a 4 μm thick ELOG layer was grown through a mask of 9 μm wide SiO_2 stripes repeated with a period of 16 μm. The SiO_2 thickness was 200 nm.

III. EXPERIMENTAL APPARATUS

The EBSD measurements on the GaN thin films of increasing thickness and all the electron channeling contrast images were acquired using an HKL Technology EBSD/forescatter system (HKL Nordlys detector with integrated forescatter system) in an LEO Supra 55VP Schottky field emission scanning electron microscope (FEG SEM) at an accelerating voltage of 20 kV and a probe current of 1 nA (unless stated otherwise in the text or in the figure captions). The EBSD measurements on the ELOG thin film were carried out with an EDAX/TSL EBSD system in a JEOL JSM6500F FEG SEM at an accelerating voltage of 20 kV and a probe current of approximately 3 nA. All EBSD patterns and electron channeling contrast images were acquired at a sample tilt of 70° (unless stated otherwise in the text or in the figure captions).

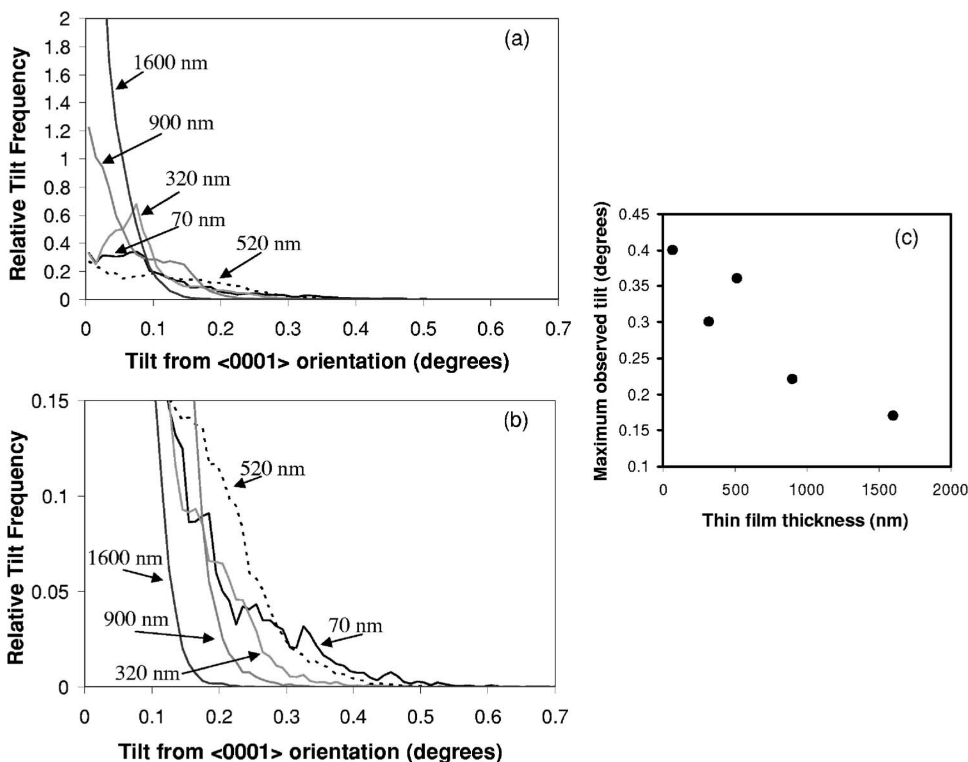

FIG. 3. (a) Relative tilt distribution for GaN thin films of increasing thickness. (b) Same as (a) but with expanded y axis. (c) Maximum tilt from the ⟨0001⟩ orientation as a function of film thickness.

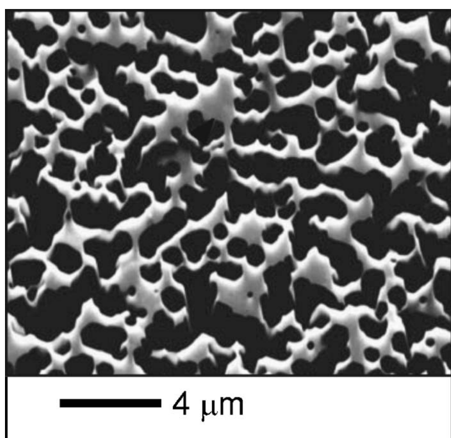

FIG. 4. Electron channeling contrast image of 320 nm GaN thin film.

IV. RESULTS AND DISCUSSION

A. EBSD tilt maps and electron channeling contrast images from GaN thin films of increasing thickness

Figure 2 shows EBSD tilt maps from an uncoalesced 70 nm GaN thin film, a partially coalesced 520 nm GaN thin film, and a fully coalesced 1600 nm GaN thin film. For the uncoalesced films, EBSD patterns were only collected from the flat top surfaces of the island grains. Figures 2(a)–2(c) [part (i)] show the EBSD tilt maps superimposed on EBSD pattern quality (also referred to as EBSD image quality[28]). As the EBSD pattern quality is dependent on sample topography, it provides an estimate of the sample topography (e.g., the topography can prevent some backscattered electrons reaching the EBSD screen leading to a poor quality EBSD pattern). Figure 2(a)–2(c) [part (ii)] show the EBSD tilt maps with the EBSD pattern quality information removed. The grey scale represents tilt away from the ideal ⟨0001⟩ orientation (in degrees). These maps clearly show that tilt in these thin films decreases as their thickness increases. Increasing the thickness of the films from 70 nm to 1600 nm results in a decrease in crystallographic tilt from $>0.4°$ to $<0.2°$. Changes in tilt of the order of 0.1° are resolvable. Figure 3 summarizes the results for all five thin films. Figures 3(a) and 3(b) show the relative frequency of a given tilt from the ⟨0001⟩ orientation versus tilt for each of the films, while Fig. 3(c) shows the maximum tilt away from the ⟨0001⟩ orientation as a function of film thickness. Figure 3(a) [and Fig. 3(c)] provides similar information to an x-ray ω scan. Figure 3 illustrates that the width of the tilt distribution decreases with increasing film thickness, except for the 520 nm film for which the tilt distribution is greater than that for the 320 nm film. The higher tilt distribution for the 520 nm film may be related to the degree of its coalescence and hence the density of voids in this film. The 70 nm film comprises three-dimensional (3D) uncoalesced islands, while the 320 nm film comprises "strings" of connected islands (see Fig. 4). The 900 nm and 1600 nm films are fully coalesced with the occasional void. In contrast, as shown in Fig. 2(b), the 520 nm film is a partially coalesced film with a high percentage of voids. On the other hand the greater tilt distribution for this film may simply be related to a small difference in growth conditions.

If a map of tilts is produced relative to a point which is significantly tilted away from the ⟨0001⟩ direction, a relative tilt map accentuating variations in tilt is produced. Figure 5 compares such a relative tilt map and an electron channeling contrast image for the 1600 nm thick film. It is possible to see correlation between features on the EBSD relative tilt map and features on the electron channeling contrast image (see features indicated by arrows for example), supporting the supposition that the contrast in the electron channeling contrast images is indeed related to orientation. The "spots" in the electron channeling contrast images correspond to threading dislocations. Note that many dislocations appear to lie on grain boundaries, i.e., they outline regions with the same grey scale and hence regions with a particular tilt.

Atomic steps terminated by the threading dislocations become more visible in the electron channeling contrast images as the backscattered electron detector is moved closer to the sample [see Figs. 6(a) and 6(b)]. The observation of atomic steps was unexpected and their appearance is discussed below.

The features present in an electron channeling contrast image and hence the information which can be extracted from it depend on the angle of the sample with respect to the impinging electron beam (i.e., sample tilt) and the position and size of the backscattered electron (or forescatter) detector. As the detector is placed closer to the sample it will intersect a wider angular range of backscattered electrons. In addition, as illustrated in Fig. 6(c), the closer the detector is to the sample, the lower the angle of backscattered electrons which will be detected. Either or both of these factors may increase the sensitivity of the backscattered electron signal to atomic steps in the sample. The wider angular range of detected backscattered electrons and/or the lower angle backscattered electrons may accentuate channeling contrast

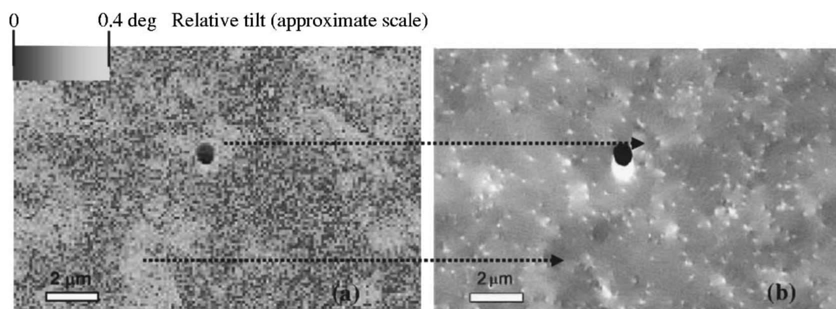

FIG. 5. (a) EBSD relative tilt map from a 1600 nm GaN thin film. (b) Electron channeling contrast image of a 1600 nm GaN thin film.

FIG. 6. (a) Electron channeling contrast image from 1600 nm GaN thin film. (b) Electron channeling contrast image from same region as (a) but with backscattered electron detector placed closer to the sample. (c) Schematic diagram illustrating that as the backscattered electron detector is moved closer to the sample: (i) it will intersect a wider angular range of backscattered electrons. (ii) it will intersect lower angle backscattered electrons. (d) Intensity profiles across dislocations situated on either side of an atomic step.

resulting from lattice distortion at the atomic steps. Alternatively, the detection of low angle backscattered electrons also enhances topographic contrast,[29] so the steps may be revealed due to enhanced topographic contrast. Finally, backscattered electrons emanating at very shallow angles from the sample surface may provide contrast similar to that obtained in scanning reflection electron microscopy (SREM) (Ref. 30) where surface resonance provides strong image contrast.

The dislocations seen in Fig. 6 must have Burgers vectors with a component out of the surface plane since they are terminating the ends of a surface step. These must therefore be threading dislocations of either screw or mixed screw-edge character. Figure 6(d) shows the intensity profiles of threading dislocations on opposite ends of an atomic step. The intensity profiles are of opposite sign, indicating dislocations where the screw component of the Burgers vector is of opposite sign.

While moving the backscattered electron detector closer to the sample enhances the contrast of the atomic steps, very little contrast change is observed for the dislocations. Figures 7(a) and 7(b) shows two electron channeling contrast images acquired at slightly different sample tilts, 69.7° and 71.0°, respectively. These small changes of tilt angle produce significant changes in the contrast of the observed dislocations. Comparing Figs. 7(a) and 7(b) reveals that there are dislocations visible in the electron channeling contrast image of Fig. 7(a) not present in the electron channeling contrast image of Fig. 7(b) (see region A for example) and vice versa. Dislocations which appear dark in Fig. 7(a) appear bright in Fig. 7(b) (see region B for example). This change in contrast for the dislocations is attributed to changes in channeling conditions with sample tilt. Further work needs to be undertaken

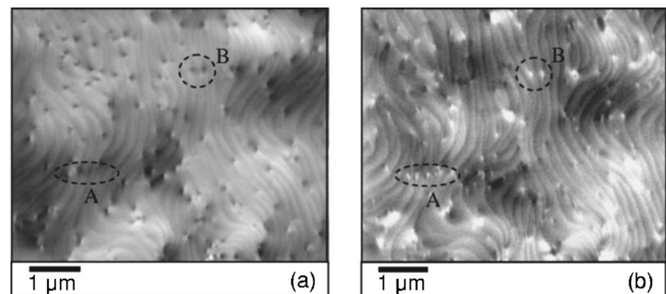

FIG. 7. (a) Electron channeling contrast image from 1600 nm GaN thin film with a sample tilt of 69.7°. (b) Electron channeling contrast image from 1600 nm GaN thin film with a sample tilt of 71.0°. Regions A and B are outlined for comparison.

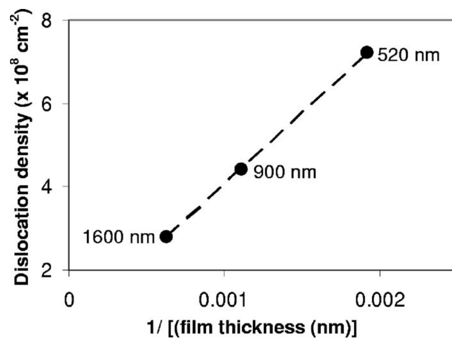

FIG. 8. Dislocation density versus 1/film thickness for GaN thin films.

to quantify the observed changes in dislocation contrast with sample tilt. As discussed above, the dislocations all appear to be associated with atomic steps on the surface, implying that few, if any are in a pure edge configuration. Previous x-ray studies have shown that there are approximately five times as many edge dislocations in this sample as screw dislocations.[31] Edge dislocations running perpendicular to the surface should be discernible due to the strain fields they produce,[32] and indeed have been imaged in FeAl by Crimp *et al.*[23] using a different geometry with the electron beam at close to normal incidence on the sample surface. The absence of threading edge dislocations from our ECCI images is probably due to a combination of the larger Burgers vector for screw ($\langle 0001 \rangle$) compared to edge threading dislocations ($1/3\langle 11-20 \rangle$)[5] in these (0001) GaN samples, and the particular (and unknown) diffraction planes excited by the incident beam. Electron channeling contrast images need to be acquired over a range of sample tilt angles together with electron channeling patterns to determine whether the observed changes in dislocation contrast can be utilized [i.e., in an analogous fashion to diffraction contrast in TEM (e.g., Refs. 33 and 34)] to obtain further information on the dislocations. Image simulations, including the effects of surface stress relaxation, should also allow a better understanding of the relative contrast produced by edge and screw dislocations for different imaging geometries.

While it is not possible to quantify the total dislocation density from the acquired electron channeling contrast images, it is possible to compare the density of visible dislocations from electron channeling contrast images acquired at the same sample tilt. Figure 8 shows the visible dislocation density versus the reciprocal of the film thickness for the 520 nm, 900 nm, and 1600 nm films, respectively. For these three films the dislocation density appears to be inversely proportional to the film thickness. It proved more difficult to acquire reliable estimates of the dislocation densities from the electron channeling contrast images of the thinner layers; this will be the subject of future work.

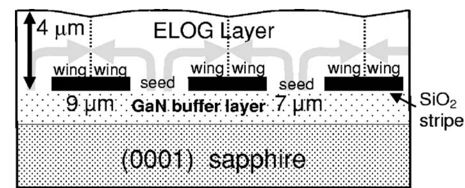

FIG. 9. Schematic diagram of cross-section of ELOG thin film. The dimensions of the ELOG thin film under study are shown.

B. EBSD and electron channeling contrast imaging of an ELOG thin film

Epitaxially laterally overgrown GaN (ELOG) thin films were developed to produce GaN with lower dislocation densities. The density of threading dislocations is reduced in ELOG to $<10^6$ cm^{-2} compared to conventional GaN thin films.[35] An ELOG thin film comprises GaN overgrown on an underlying GaN epitaxial buffer layer patterned with a SiO_2 or SiN_x striped mask (SiO_2 in the present case). GaN growth is seeded by the GaN buffer layer and grows laterally over the SiO_2 mask; this is illustrated in Fig. 9. The material above the mask (wing regions) has a lower threading dislocation density than that above the seed region, as the majority of the dislocations propagate vertically in the seed region. Some dislocations do bend at the interface and propagate parallel to SiO_2 mask, producing a tilt in the wing region of up to a few degrees.[36] It is this wing tilt that we investigate here with EBSD and electron channeling contrast imaging.

An electron channeling contrast image of our ELOG thin film graphically illustrates the tilt in the film. Figure 10 compares an electron channeling contrast image and a secondary electron image from our ELOG thin film. The stripes are not visible in the secondary electron image; however the tilt in the film unequivocally reveals the stripes in the electron channeling contrast image. The intensity profile shown in the

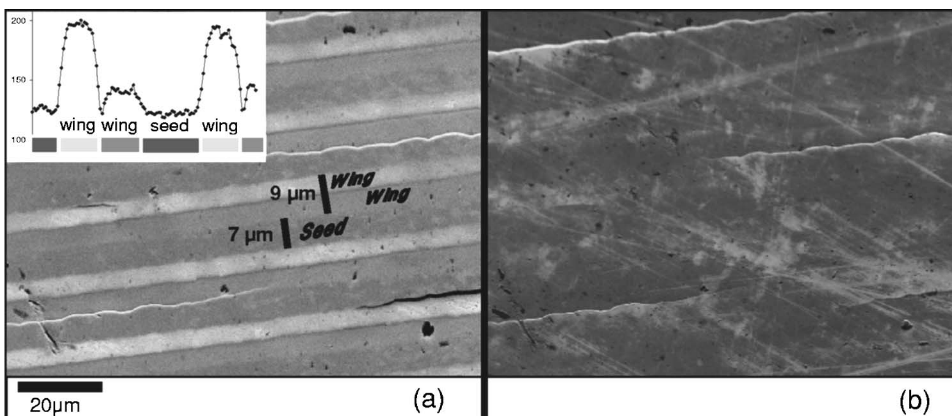

FIG. 10. (a) Electron channeling contrast image from ELOG thin film. (b) Secondary electron image from same region of ELOG film as (a). The inset in (a) is an intensity profile across the electron channeling contrast image.

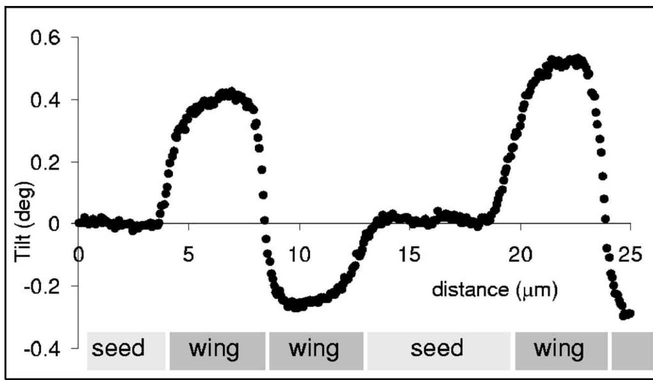

FIG. 11. Variation in tilt across the ELOG thin film.

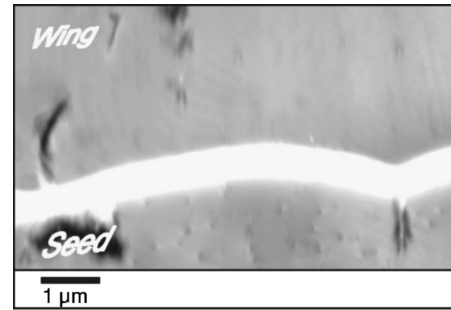

FIG. 12. High magnification electron channeling contrast image from ELOG thin film (acquired at 15 kV).

inset of Fig. 10(a) is a qualitative measure of the variation of tilt in the film; however, the relative brightness of the stripes and hence the intensity profile will change with sample tilt and the position of the backscattered electron detector. On the other hand, EBSD can provide a quantitative measure of tilt.

To obtain the necessary sensitivity to measure variations in tilt across the ELOG thin film, we apply a method developed to allow small spatial variations of elastic strain and lattice rotation to be determined from a series of EBSD patterns.[12] In the present work EBSD patterns were recorded with the usual large ≈60° capture angle subtended by the screen at the sample. A series of EBSD patterns were recorded along a line scan on the top surface of the ELOG thin film running perpendicular to the SiO_2 stripe direction. EBSD pattern shifts were measured at four distinct regions on the screen. Rigid body rotations (and elastic strains) can be determined from analysis of the four measured pattern shifts. Here we show only the variation in tilt (i.e., rotation about an axis parallel to the SiO_2 stripes, Fig. 11) across the ELOG thin film.

Changes in tilt of the order of 0.02° are resolvable from the EBSD line profile. The intensity profile obtained from the electron channeling contrast image as shown in the inset of Fig. 10(a) is qualitatively similar to the quantitative variation in tilt derived from EBSD measurements as shown in Fig. 11. The electron channeling contrast intensity profile appears to be rectified when compared to the EBSD profile.

Finally, Fig. 12 shows a high magnification electron channeling contrast image from the ELOG thin film. Note that the dislocation density appears to be less in the wing region.

V. CONCLUSIONS AND FUTURE WORK

In conclusion we hope we have shown that EBSD and electron channeling contrast imaging are useful techniques for characterizing nitride thin films. Future work includes: (1) using EBSD to quantify twist in addition to tilt in nitride thin films; (2) acquiring electron channeling contrast images as a function of sample tilt and as a function of backscattered electron detector size and position, together with electron channeling patterns to establish whether electron channeling contrast imaging can be used to identify dislocations and determine their total density in nitride thin films.

ACKNOWLEDGMENT

The authors are grateful for the support of the UK Engineering and Physical Sciences Research Council.

[1] G. Zorpette, Sci. Am. **283**, 19 (2000).
[2] A. Hangleiter, MRS Bull. **28**, 350 (2003).
[3] L. F. Eastman, IEEE Spectrum, May 2002. http://www.spectrum.ieee.org/WEBONLY/publicfeature/may02/gani.html
[4] E. Piner, Compound Semicond. **10**, 27 (2004).
[5] S. K. Mathis, A. E. Romanov, L. F. Chen, G. E. Belz, W. Pompe, and J. S. Speck, Phys. Status Solidi A **179**, 125 (2000).
[6] H. Marchand, X. H. Wu, J. P. Ibbetson, P. T. Fini, P. Kozodoy, S. Keller, J. S. Speck, S. P. DenBaars, and U. K. Mishra, Appl. Phys. Lett. **73**, 747 (1998).
[7] F. J. Humphreys, Y. Huang, I. Brough, and C. Harris, J. Microsc. **195**, 212 (1999).
[8] C. Trager-Cowan, S. K. Manson-Smith, D. A. Cowan, F. Sweeney, D. McColl, A. Mohammed, R. Timm, P. G. Middleton, K. P. O'Donnell, D. Zubia, and S. D. Hersee, Mater. Sci. Eng., B **B82**, 19 (2001).
[9] D. J. Dingley and V. Randle, J. Mater. Sci. **27**, 4545 (1992).
[10] D. Prior, A. Boyle, F. Brenker, M. Cheadle, A. Day, G. Lopez, L. Peruzzo, G. Potts, S. Reddy, R. Spiess, N. Timms, P. Trimby, J. Wheeler, and L. Zetterström, Am. Mineral. **84**, 1741 (1999).
[11] V. Randle, *Microtexture determination and its applications* (The Inst. of Materials, London, 1992).
[12] A. J. Wilkinson, J. Electron Microsc. **49**, 299 (2000).
[13] K. Z. Troost, P. Van Der Sluis, and D. J. Gravesteijn, Appl. Phys. Lett. **62**, 1110 (1993).
[14] K. Z. Baba-Kishi, J. Appl. Crystallogr. **24**, 38 (1991).
[15] C. Trager-Cowan, F. Sweeney, J. Hastie, S. K. Manson-Smith, D. A. Cowan, D. McColl, A. Mohammed, K. P. O'Donnell, D. Zubia, S. D. Hersee, C. T. Foxon, I. Harrison, and S. V. Novikov, J. Microsc. **205**, 226 (2002).
[16] C. Trager-Cowan, F. Sweeney, A. J. Wilkinson, I. M. Watson, P.

G. Middleton, K. P. O'Donnell, D. Zubia, S. D. Hersee, S. Einfeldt, and D. Hommel, Phys. Status Solidi C **0**, 532 (2002).
[17] R. P. Goehner and J. R. Michael, J. Res. Natl. Inst. Stand. Technol. **101**, 301 (1996).
[18] P. Morin, M. Pitavel, D. Besnard, and G. Fontaine, Philos. Mag. A **40**, 511 (1979).
[19] D. C. Joy, D. E. Newbury, and D. L. Davidson, J. Appl. Phys. **53**, R81 (1982).
[20] J. T. Czernuska, N. J. Long, E. D. Boyes, and P. B. Hirsch, Philos. Mag. Lett. **62**, 227 (1990).
[21] A. J. Wilkinson and P. B. Hirsch, Micron **28**, 279 (1997).
[22] B. A. Simpkin and M. A. Crimp, Ultramicroscopy **77**, 65 (1999).
[23] M. A. Crimp, B. A. Simkin, and B. C. Ng, Philos. Mag. Lett. **81**, 833 (2001).
[24] D. J. Prior, P. W. Trimby, U. D. Weber, and D. J. Dingley, Miner. Mag. **60**, 859 (1996).
[25] D. Prior, A. Boyle, F. Brenker, M. Cheadle, A. Day, G. Lopez, L. Peruzzo, G. Potts, S. Reddy, R. Spiess, N. Timms, P. Trimby, J. Wheeler, and L. Zetterström, Am. Mineral. **84**, 1741 (1999).
[26] A. P. Day and T. E. Quested, J. Microsc. **195**, 186 (1999).
[27] I. M. Watson, C. Liu, K. S. Kim, H.-S. Kim, C. J. Deatcher, J. M. Girkin, M. D. Dawson, P. R. Edwards, C. Trager-Cowan, and R. W. Martin, Phys. Status Solidi A **188**, 743 (2001).
[28] S. J. Wright and M. M. Nowell, Microsc. Microanal. **12**, 72 (2006).
[29] O. C. Wells, Appl. Phys. Lett. **16**, 151 (1970).
[30] Z. L. Wang, Rep. Prog. Phys. **56**, 997 (1993).
[31] T. A. Lafford, P. J. Parbrook, and B. K. Tanner, Phys. Status Solidi C **0**, 542 (2002).
[32] A. J. Wilkinson, Philos. Mag. Lett. **73**, 337 (1996).
[33] D. M. Follstaedt, N. A. Milssert, D. D. Koleske, C. C. Mitchell, and K. C. Cross, Appl. Phys. Lett. **83**, 4797 (2003).
[34] R. Datta, M. J. Kappers, J. S. Barnard, and C. J. Humphreys, Appl. Phys. Lett. **85**, 3411 (2004).
[35] S. Nakamura, M. Senoh, S. Nagahama, N. Iwasa, T. Matushita, and T. Mukai, MRS Internet J. Nitride Semicond. Res. **4S1**, G1.1 (1999).
[36] N. Gmeinwieser, K. Engl, P. Gottfriedsen, U. T. Schwarz, J. Zweck, W. Wegscheider, S. Miller, H.-J. Lugauer, A. Leber, A. Weimar, A. Lell, and V. Härle, J. Appl. Phys. **96**, 3666 (2004).